

Theory of Mixed-State Effect on Quasiparticle Interference in Iron-based Superconductors

Yi Gao,¹ Huaixiang Huang,² and Peiqing Tong¹

¹*Department of Physics and Institute of Theoretical Physics,
Nanjing Normal University, Nanjing, Jiangsu, 210046, China*

²*Department of Physics, Shanghai University, Shanghai 200444, China*

Based on a phenomenological model with s_{\pm} or s -wave pairing symmetry, the mixed-state effect on quasiparticle interference in iron-based superconductors is investigated by solving large-scale Bogoliubov-de Gennes equations based on the Chebyshev polynomial expansion. Taking into account the presence of magnetic field, our result for the s_{\pm} pairing is in qualitative agreement with recent scanning tunneling microscopy experiment while for the s -wave pairing, the result is in apparent contradiction with experimental observations, thus excluding the s -wave pairing. Furthermore, we treat the effect of vortices rigorously instead of approximating the vortices as magnetic impurities, thus our results are robust and should be more capable of explaining the experimental data.

PACS numbers: 74.70.Xa, 74.55.+v, 74.25.Op, 74.25.Ha

Introduction.—The discovery of iron-based superconductors [1] has triggered efforts to elucidate the superconducting (SC) pairing mechanism in these materials. One hotly debated issue is the symmetry and structure of the SC gap. Theoretically, it was initially suggested that the pairing may be established via spin fluctuations, leading to the so-called s_{\pm} pairing symmetry ($\Delta_{\mathbf{k}} \sim \cos k_x + \cos k_y$ defined in the 2Fe/cell Brillouin zone). In this case the SC order parameter (OP) exhibits a sign reversal between the hole pockets (around the Γ point) and electron pockets (around the M point) [2]. Later, s -wave pairing symmetry without sign reversal was also proposed to be a possible candidate which is induced by orbital fluctuations due to the electron-phonon interaction [3]. Experimentally, the results about the pairing symmetry remain highly controversial as well. For example, in $\text{Ba}_{0.6}\text{K}_{0.4}\text{Fe}_2\text{As}_2$, an optimally hole-doped iron-based superconductor [4], the SC gaps measured by the angle resolved photoemission spectroscopy can be approximately fitted by $|\Delta_{\mathbf{k}}| \sim |\cos k_x + \cos k_y|$, with almost isotropic gaps on all the Fermi surfaces (FS) [5], indicating the possible pairing symmetry to be either s_{\pm} or s -wave. Neutron scattering experiments observed a resonance peak at $\mathbf{Q} = (\pi, \pi)$ below the SC transition temperature [6] as predicted by some theoretical works assuming s_{\pm} symmetry [7], thus at first glance they seemed to support each other. However, later theoretical works suggested that the experimentally observed resonance peak can also be reproduced by assuming s -wave pairing [8].

Recently, in order to clarify the pairing symmetry, Hanaguri *et al.* used scanning tunneling microscopy (STM) to image the quasiparticle interference (QPI) patterns in the SC state [9]. They proposed that the relative sign of the SC OP can be determined from the magnetic-field dependence of quasiparticle scattering amplitudes and claimed that their experimental data were only consistent with the s_{\pm} scenario but not the s -wave one. Soon

after, the experimental results were put into question and argued instead to arise from the Bragg scattering but not due to the QPI because the observed peaks are too sharp [10]. On the other hand, the magnetic field will induce vortices into the system and lead to the inhomogeneity of the pairing OP in real space, thus affecting the QPI patterns. Theoretical analyzes performed previously have investigated the mixed-state effect on the QPI [11–13]. However, in Ref. [11], only amplitude suppression of the OP near the vortex core was considered, without taking into account the phase variation. In Ref. [12], the mixed-state effect was treated by using quasiclassical approximation and the QPI derived in this way was rather broad compared to the experimental observation. Furthermore, in Ref. [13], only the effect of the Zeeman splitting was considered, which should be negligible with respect to the mixed-state effect. Thus there still lacks direct theoretical confirmation of the mixed-state effect on the QPI.

Therefore in this work we adopt a phenomenological model with s_{\pm} pairing symmetry to study the influence of vortices on the QPI by directly solving large-scale Bogoliubov-de Gennes (BdG) equations in real space based on the Chebyshev polynomial expansion. For comparison, the problem is also studied for s -wave pairing. In this way the mixed-state effect on the QPI can be rigorously investigated and the results unambiguously support s_{\pm} pairing symmetry in iron-based superconductors.

Method.—We begin with an effective two-orbital model on a two-dimensional lattice [14], with a phenomenological form for the intraorbital pairing terms. The Hamiltonian can be written as

$$H = - \sum_{ij, \alpha\beta, \sigma} [t'_{ij, \alpha\beta} + (\mu - V_{imp} \delta_{iimp}) \delta_{ij} \delta_{\alpha\beta}] c_{i\alpha\sigma}^{\dagger} c_{j\beta\sigma} + \sum_{ij, \alpha\beta} (\Delta_{ij, \alpha\beta} c_{i\alpha\uparrow}^{\dagger} c_{j\beta\downarrow}^{\dagger} + H.c.). \quad (1)$$

Here i and j are the site indices while $\alpha, \beta = 1, 2$ are the orbital ones. σ represents the spin and μ is the chemical potential. Then we consider potential scattering by nonmagnetic impurities through V_{imp} with i_{imp} being the locations of the impurities. $\Delta_{ij,\alpha\beta} = \frac{V_{ij}\delta_{\alpha\beta}}{2}(\langle c_{j\beta\downarrow}c_{i\alpha\uparrow} \rangle - \langle c_{j\beta\uparrow}c_{i\alpha\downarrow} \rangle)$ is the intraorbital spin singlet bond OP, where V_{ij} is the onsite [$i = j$] or next-nearest-neighbor [$i = j \pm (\hat{x} \pm \hat{y})$] attraction which we choose to achieve the s -wave or s_{\pm} pairing symmetry, respectively. In the presence of a magnetic field B perpendicular to the plane, the hopping integral can be expressed as $t'_{ij,\alpha\beta} = t_{ij,\alpha\beta} \exp[i \frac{\pi}{\Phi_0} \int_j^i \mathbf{A}(\mathbf{r}) \cdot d\mathbf{r}]$, where $\Phi_0 = hc/2e$ is the SC flux quantum, and $\mathbf{A} = (-By, 0, 0)$ is the vector potential in the Landau gauge. The hopping integrals are

$$t_{ij,\alpha\beta} = \begin{cases} t_1 & \alpha = \beta, i = j \pm \hat{x}(\hat{y}), \\ \frac{1+(-1)^j}{2}t_2 + \frac{1-(-1)^j}{2}t_3 & \alpha = \beta, i = j \pm (\hat{x} + \hat{y}), \\ \frac{1+(-1)^j}{2}t_3 + \frac{1-(-1)^j}{2}t_2 & \alpha = \beta, i = j \pm (\hat{x} - \hat{y}), \\ t_4 & \alpha \neq \beta, i = j \pm (\hat{x} \pm \hat{y}), \\ 0 & \text{otherwise.} \end{cases} \quad (2)$$

The Chebyshev polynomials can be written as $\phi_k(x) = \cos[k \arccos x]$ and satisfy

$$\phi_0(x) = 1, \phi_1(x) = x, \phi_k(x) = 2x\phi_{k-1}(x) - \phi_{k-2}(x),$$

$$\sum_{k=0}^{\infty} \frac{W(x)}{\nu_k} \phi_k(x) \phi_k(x') = \delta(x - x'), \quad (3)$$

where $W(x) = 1/\sqrt{1-x^2}$, $\nu_k = \pi(1 + \delta_{k0})/2$ and $x \in [-1, 1]$. Next we define the Green's function matrix:

$$G(\tau) = -\langle T\tau C(\tau)C^\dagger(0) \rangle, \quad (4)$$

with $C^\dagger = (\cdots, c_{j1\uparrow}^\dagger, c_{j2\uparrow}^\dagger, \cdots, c_{j1\downarrow}, c_{j2\downarrow}, \cdots)$. Eq. (1) can be diagonalized as

$$H = C^\dagger M C = C^\dagger Q Q^\dagger M Q Q^\dagger C = \Phi^\dagger D \Phi. \quad (5)$$

Here Q is a unitary matrix that satisfies $(Q^\dagger M Q)_{rs} = D_{rs} = \delta_{rs} E_s$ and the spectral function can be expressed as [15]

$$\begin{aligned} d_{rs}(\omega) &= -\frac{1}{2\pi i} [G_{rs}(\omega + i\eta) - G_{rs}(\omega - i\eta)] \\ &= \sum_{\gamma} Q_{r\gamma} Q_{s\gamma}^* \delta(\omega - E_{\gamma}) = \frac{1}{a} \sum_{\gamma} Q_{r\gamma} Q_{s\gamma}^* \delta(\tilde{\omega} - \xi_{\gamma}) \\ &= \frac{1}{a} \sum_{\gamma} Q_{r\gamma} Q_{s\gamma}^* \sum_{k=0}^{\infty} \frac{W(\tilde{\omega})}{\nu_k} \phi_k(\tilde{\omega}) \phi_k(\xi_{\gamma}) \end{aligned}$$

$$= \frac{1}{a} \sum_{k=0}^{\infty} \frac{W(\tilde{\omega})}{\nu_k} \phi_k(\tilde{\omega}) \phi_k(\tilde{M})_{rs},$$

$$d(\omega) = \frac{1}{a} \sum_{k=0}^{\infty} \frac{W(\tilde{\omega})}{\nu_k} \phi_k(\tilde{\omega}) \phi_k(\tilde{M}). \quad (6)$$

Here $r, s, \gamma = 1, \cdots, L$ with $L = 4N_x N_y$ and N_x (N_y) being the number of lattice sites along \hat{x} (\hat{y}) direction of the 2D lattice. $a = (E_{\gamma}^{max} - E_{\gamma}^{min})/(2 - \epsilon)$ ($\epsilon > 0$ is a small number), $b = (E_{\gamma}^{max} + E_{\gamma}^{min})/2$, $\tilde{\omega} = (\omega - b)/a$, $\xi_{\gamma} = (E_{\gamma} - b)/a$ and $\tilde{M} = (M - bI)/a$.

If we further define the L -dimensional vectors $e(o)$ and $h(o)$ as $e(o)_{\gamma} = \delta_{\gamma o}$ and $h(o)_{\gamma} = \delta_{\gamma o+2N_s}$ ($N_s = N_x N_y$ and $o = 1, \cdots, 2N_s$), we can express the self-consistent parameters as

$$n_{j\beta\uparrow} = \langle c_{j\beta\uparrow}^\dagger c_{j\beta\uparrow} \rangle = \int_{-\infty}^{\infty} d\omega f(\omega) d_{mm}(\omega)$$

$$= \int_{-\infty}^{\infty} d\omega f(\omega) e(m)^T d(\omega) e(m)$$

$$= \sum_{k=0}^{N-1} g_k e(m)^T e_k(m) \frac{T_k}{\nu_k},$$

$$n_{j\beta\downarrow} = 1 - \sum_{k=0}^{N-1} g_k h(m)^T h_k(m) \frac{T_k}{\nu_k},$$

$$\Delta_{ij,\alpha\beta} = \frac{V_{ij}\delta_{\alpha\beta}}{2} \sum_{k=0}^{N-1} g_k [e(n)^T h_k(m) + e(m)^T h_k(n)] \frac{T_k}{\nu_k}, \quad (7)$$

where $m = 2(j_y + N_y j_x) + \beta$ and $n = 2(i_y + N_y i_x) + \alpha$ with $i_x, j_x = 0, \cdots, N_x - 1$ and $i_y, j_y = 0, \cdots, N_y - 1$. $e_k(m) = \phi_k(\tilde{M})e(m)$, $h_k(m) = \phi_k(\tilde{M})h(m)$ and $T_k = \int_{-1}^1 d\tilde{\omega} f(a\tilde{\omega} + b) W(\tilde{\omega}) \phi_k(\tilde{\omega})$. N is the cutoff in the summation and g_k is the kernel we convolute to avoid Gibbs oscillations [16]. In addition, $f(x)$ is the Fermi distribution function. At zero temperature we have

$$T_k = \begin{cases} \pi - \arccos(-\frac{b}{a}) & k = 0, \\ -\frac{\sin[k \arccos(-\frac{b}{a})]}{k} & k \neq 0. \end{cases} \quad (8)$$

Then we can solve the BdG equations self-consistently and the chemical potential is determined by the doping concentration. The calculation is repeated until the absolute error of the OP between two consecutive iteration

steps and that of the total electron number are less than 10^{-4} . The local density of states (LDOS) is given by

$$\rho_j(\omega) = \frac{1}{a} \sum_{\beta} \sum_{k=0}^{N-1} \frac{g_k}{\nu_k} [W(\tilde{\omega}) \phi_k(\tilde{\omega}) e(m)^T e_k(m) + W(\tilde{\omega}') \phi_k(\tilde{\omega}') h(m)^T h_k(m)], \quad (9)$$

where $\tilde{\omega}' = (-\omega - b)/a$.

The benefits of this method are threefold. First, it requires much less storage than the exact diagonalization method since the matrix M is sparse, thus we can solve large-scale BdG equations and obtain the QPI by Fourier transforming the real-space LDOS in sufficiently wide range. Second, it is applicable in parallel computation because the self-consistent parameters on each lattice site can be calculated separately. Third, the expansion scheme is very stable and efficient.

In our calculation, the magnitudes of the parameters are chosen as $t_{1-4} = 1, 0.4, -2, 0.04$. Magnetic unit cells are introduced where each unit cell accommodates four SC flux quanta and the linear dimension is $N_x \times N_y = 80 \times 80$, corresponding to a magnetic field $B \approx 8.32$ Tesla, close to the experimental value (10 Tesla) [9]. V_{ii} and V_{ij} [$i = j \pm (\hat{x} \pm \hat{y})$] are chosen to be -2.8 and -2 , respectively. Moreover we introduce 12 randomly distributed impurities with $V_{imp} = 0.3$. E_{γ}^{max} (E_{γ}^{min}) is chosen as 1.5 (-1.5) band width. Throughout the paper, we set the system to be 20% hole-doped. In calculating the self-consistent parameters, we use the Jackson kernel

$$g_k = \frac{(N - k + 1) \cos \frac{\pi k}{N+1} + \sin \frac{\pi k}{N+1} \cot \frac{\pi}{N+1}}{N + 1}, \quad (10)$$

with $\epsilon = 0.001$ and $N = 500$. For the LDOS we convolute the Lorentz kernel

$$g_k = \frac{\sinh[\lambda(1 - \frac{k}{N})]}{\sinh \lambda}, \quad (11)$$

with $\lambda = 4$, $\epsilon = 0.004$ and $N = \lambda/\epsilon$.

Results and discussion.—First we consider the s_{\pm} case. For $V_{imp} = 0$, Fig. 1(a) shows that there exists a negative-energy in-gap peak in the LDOS at the vortex core center, in agreement with the experimental observation [17] and our previous results based on the exact diagonalization method [18], indicating the reliability of the Chebyshev polynomial-expansion scheme. Figure 1(c) plots the spatial distribution of $Z_j(\omega) = \rho_j(\omega)/\rho_j(-\omega)$ as defined in Ref. [9], for $B = 0$ and at $\omega = \Delta$. The locations of the impurities can be clearly identified as the low-intensity spots. The corresponding $Z_{\mathbf{q}}(\omega)$, which is the Fourier transformation of $Z_j(\omega)$, is shown in Fig. 1(d). We notice that there are high-intensity peaks at \mathbf{q}_2 [$(\pm\pi, 0)$ and $(0, \pm\pi)$] which arise from the inter-pocket scattering between the hole and electron pockets.

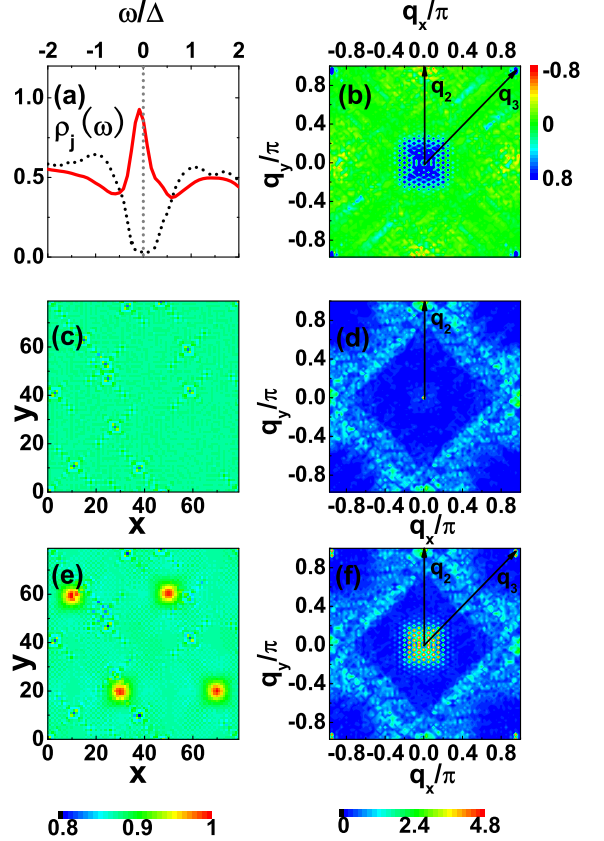


FIG. 1: (color online) (a) The LDOS at the vortex core center (red solid) and at $B = 0$ (black dot) as a function of the reduced energy ω/Δ . Here 2Δ is the SC gap between two SC coherence peaks in the LDOS at $B = 0$. The gray-dotted line indicates the position of $\omega = 0$. (b) $Z_{\mathbf{q}}(B \neq 0) - Z_{\mathbf{q}}(B = 0)$ at $\omega = \Delta$. (c) and (d) show $Z_j(\omega = \Delta)$ and $Z_{\mathbf{q}}(\omega = \Delta)$ at $B = 0$, respectively. (e) and (f) are the same as (c) and (d), respectively, but for $B \neq 0$. (c) and (e) share the same color scale while the case is similar for (d) and (f).

Furthermore the intensities at \mathbf{q}_3 [$(\pm\pi, \pm\pi)$] are much weaker than those at \mathbf{q}_2 , consistent with the experimental observation [9]. Upon applying the magnetic field, vortices are introduced into the system and their locations are denoted as the high-intensity spots in Fig. 1(e). In this case, from Fig. 1(f) we can see that there exist additional peaks at \mathbf{q}_3 , whose intensities are enhanced by the application of the magnetic field and they are due to the inter-pocket scattering between different electron pockets (see Fig. 1 in Ref. [9]). Figure 1(b) shows the magnetic field-induced change in the QPI intensities defined as $Z_{\mathbf{q}}(B \neq 0) - Z_{\mathbf{q}}(B = 0)$. In the presence of the time-reversal symmetry breaking due to the magnetic field, the sign-preserving scatterings at \mathbf{q}_3 (\mathbf{q}_3 connects the FS with the same sign of the SC OP) are enhanced while the sign-reversing scatterings at \mathbf{q}_2 (\mathbf{q}_2 connects the FS with the opposite sign of the SC OP) are suppressed. Both

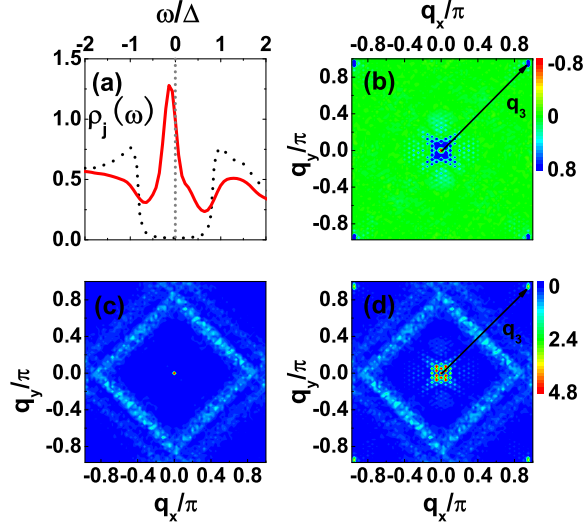


FIG. 2: (color online) (a), (b), (c) and (d) are similar to Figs. 1(a), 1(b), 1(d) and 1(f), respectively. (c) and (d) share the same color scale.

the locations and the sharpness of the QPI peaks shown in Figs. 1(b), 1(d) and 1(f) are in reasonable agreement with the experimental data [9], suggesting that the experimentally observed peaks are indeed due to the QPI but not the Bragg scattering as argued in Ref. [10].

Next we consider the s -wave case. For $V_{imp} = 0$, the LDOS at $B = 0$ (black dot) and at the vortex core center (red solid) shown in Fig. 2(a) are also consistent with those obtained by exact diagonalization [19], again suggesting the validity of the current polynomial-expansion scheme. From Fig. 2(c) we notice, the QPI in the presence of impurities at $B = 0$ exhibits no pronounced peaks at either q_2 or q_3 , as compared to the clear peaks at q_2 in the s_{\pm} case as shown in Fig. 1(d). After applying the magnetic field, the intensities at q_3 are enhanced and they form sharp peaks as shown in Fig. 2(d), similar to the s_{\pm} case. At last, from the magnetic field-induced change in the QPI intensities plotted in Fig. 2(b) we can see, the intensities are enhanced at q_3 but remain almost unchanged at q_2 . The lack of distinct structures at q_2 is in stark contrast to the s_{\pm} case and is inconsistent with the experimental observations [9]. Therefore, the different behavior of the QPI intensities at q_2 in the s_{\pm} and s -wave pairing cases makes it possible to distinguish these two types of pairing symmetry since the STM experiment observed clear structures at q_2 , thus excluding the possibility of s -wave pairing in iron-based superconductors.

Summary.—In summary, by using the Chebyshev polynomial expansion to directly solve large-scale BdG equa-

tions in real space, we have investigated the mixed-state effect on QPI in iron-based superconductors by assuming s_{\pm} or s -wave pairing symmetry. For the s_{\pm} pairing, the QPI intensities at q_2 which connects the FS with the opposite sign of the SC OP are suppressed by the application of the magnetic field while the situation at q_3 is reversed where q_3 connects the FS with the same sign of the SC OP. The obtained results at both $B = 0$ and $B \neq 0$ are in qualitative agreement with experiment, suggesting that the experimentally observed peaks are indeed due to QPI. On the other hand, for the s -wave pairing, the QPI intensities at q_2 are featureless both with and without the magnetic field. Based on the available experimental data, the s -wave pairing can be excluded in iron-based superconductors.

Acknowledgments We thank A. Li, D. G. Zhang, T. Zhou, C. S. Ting and Y. Xiong for helpful discussions. This work was supported by the National Natural Science Foundation of China (Grants No. 10974097 and No. 11175087), and by National Key Projects for Basic Research of China (Grant No. 2009CB929501).

-
- [1] Y. Kamihara *et al.*, J. Am. Chem. Soc. **130**, 3296 (2008).
 - [2] I. I. Mazin *et al.*, Phys. Rev. Lett. **101**, 057003 (2008); A. V. Chubukov, M. G. Vavilov, and A. B. Vorontsov, Phys. Rev. B **80**, 140515(R) (2009).
 - [3] H. Kontani and S. Onari, Phys. Rev. Lett. **104**, 157001 (2010).
 - [4] M. Rotter, M. Tegel, and D. Johrendt, Phys. Rev. Lett. **101**, 107006 (2008).
 - [5] H. Ding *et al.*, Europhys. Lett. **83**, 47001 (2008); K. Nakayama *et al.*, Europhys. Lett. **85**, 67002 (2009).
 - [6] A. D. Christianson *et al.*, Nature **456**, 930 (2008); S. Chi *et al.*, Phys. Rev. Lett. **102**, 107006 (2009); Y. Qiu *et al.*, Phys. Rev. Lett. **103**, 067008 (2009); D. S. Inosov *et al.*, Nature Physics, **6**, 178 (2010).
 - [7] T. A. Maier and D. J. Scalapino, Phys. Rev. B **78**, 020514 (2008); M. M. Korshunov and I. Eremin, Phys. Rev. B **78**, 140509 (2008).
 - [8] S. Onari *et al.*, Phys. Rev. B **81**, 060504 (2010); S. Onari and H. Kontani, Phys. Rev. B **84**, 114518 (2011);
 - [9] T. Hanaguri *et al.*, Science **328**, 474 (2010).
 - [10] I. I. Mazin and D. J. Singh, arXiv:1007.0047.
 - [11] E. Plamadeala *et al.*, Phys. Rev. B **81**, 134513 (2010).
 - [12] Y. Nagai and Y. Kato, Phys. Rev. B **82**, 174507 (2010).
 - [13] S. Sykora and P. Coleman, Phys. Rev. B **84**, 054501 (2011).
 - [14] Degang Zhang, Phys. Rev. Lett. **103**, 186402 (2009).
 - [15] Y. Nagai *et al.*, J. Phys. Soc. Jpn. **81**, 024710 (2012).
 - [16] A. Weiße *et al.*, Rev. Mod. Phys. **78**, 275 (2006).
 - [17] L. Shan *et al.*, Nature Phys. **7**, 325 (2011).
 - [18] Y. Gao *et al.*, Phys. Rev. Lett. **106**, 027004 (2011).
 - [19] Y. Gao *et al.*, Phys. Rev. B **84**, 224509 (2011).